21. S. R. Leone *et al.*, *Nat. Photonics* **8**, 162–166 (2014).
22. Á. Jiménez-Galán, L. Argenti, F. Martín, *Phys. Rev. Lett.* **113**, 263001 (2014).
23. A. Jiménez-Galán, F. Martín, L. Argenti, *Phys. Rev. A* **93**, 023429 (2016).
24. Z. X. Zhao, C. D. Lin, *Phys. Rev. A* **71**, 060702 (2005).
25. See supplementary materials on *Science* Online.
26. A. E. Miroshnichenko, S. Flach, Y. S. Kivshar, *Rev. Mod. Phys.* **82**, 2257–2298 (2010).
27. A. S. Sandhu *et al.*, *Science* **322**, 1081–1085 (2008).
28. J. Caillat *et al.*, *Phys. Rev. Lett.* **106**, 093002 (2011).
29. P. Hockett, E. Frumker, D. M. Villeneuve, P. B. Corkum, *J. Phys. B* **49**, 095602 (2016).
30. Y. Mairesse *et al.*, *Science* **302**, 1540–1543 (2003).

ACKNOWLEDGMENTS

We thank S. Weber for crucial contributions to the PLFA attosecond beamline; D. Cubaynes, M. Meyer, F. Penent, and J. Palaudoux for setup and testing of the electron spectrometer; and O. Smirnova for fruitful discussions. Supported by European Union grant H2020-MSCA-ITN-MEDEA-641789, Agence Nationale de la Recherche grants ANR-15-CE30-0001-01-CIMBAAD and ANR11-EQPX0005-ATTOLAB, European Research Council advanced grant XCHEM 290853, European COST Action grant XLIC CM1204, and MINECO Project grant FIS2013-42002-R. We acknowledge allocation of computer time from CCC-UAM and Mare Nostrum BSC.

SUPPLEMENTARY MATERIALS

www.sciencemag.org/content/354/6313/734/suppl/DC1
Supplementary Text
Figs. S1 to S7
Movie S1
References (*31*–*43*)

8 July 2016; accepted 5 October 2016
10.1126/science.aah5188

CHEMICAL PHYSICS

Observing the ultrafast buildup of a Fano resonance in the time domain

A. Kaldun,[1]*† A. Blättermann,[1]† V. Stooß,[1] S. Donsa,[2] H. Wei,[3] R. Pazourek,[2] S. Nagele,[2] C. Ott,[1] C. D. Lin,[3] J. Burgdörfer,[2] T. Pfeifer[1,4]‡

Although the time-dependent buildup of asymmetric Fano line shapes in absorption spectra has been of great theoretical interest in the past decade, experimental verification of the predictions has been elusive. Here, we report the experimental observation of the emergence of a Fano resonance in the prototype system of helium by interrupting the autoionization process of a correlated two-electron excited state with a strong laser field. The tunable temporal gate between excitation and termination of the resonance allows us to follow the formation of a Fano line shape in time. The agreement with ab initio calculations validates our experimental time-gating technique for addressing an even broader range of topics, such as the emergence of electron correlation, the onset of electron-internuclear coupling, and quasi-particle formation.

Fano resonances generally occur in the course of excitation of discrete quantum states embedded in and coupled to a continuum (*1*, *2*). As such, they play a fundamental role in nuclear, atomic, molecular, and condensed-matter physics as well as photonics (*3*–*12*). In the prominent example of helium, the discrete doubly excited states are located within different sets of continua, where the prominent 2s2p state is coupled only to the continuum of singly ionized ground-state Helium He^+ (1s). Coulomb interaction among the two electrons leads to autoionization, thus coupling the discrete state and the 1s continuum and giving rise to the famous asymmetric Fano line profiles. Following the early scientific work on attosecond dynamics in laser-driven helium (*13*, *14*), several recent theoretical calculations have predicted the time-dependent formation of Fano resonances (*15*–*20*). However, up to now no such experiment has been performed.

Here, we report a measurement of the time-dependent formation of a Fano resonance in the prototype system of helium. We observed the transient buildup of the 2s2p doubly excited state via extreme ultraviolet (XUV) absorption spectroscopy using high-harmonic radiation. Monitoring the formation of the Fano line was achieved by rapidly terminating the coherent dipole response of the atom via saturated strong-field ionization (SFI) by use of an intense near-infrared (NIR) laser pulse. The key idea is that the NIR pulse acts as a temporal gate of the Fano resonance decay. By varying the time delay between the XUV and the NIR pulse with subfemtosecond precision, we tracked the evolution of the Fano line shape in real time (Fig. 1). To that end, we used laser intensities beyond the Fano-phase control regime discussed in previous work (*7*) to fully deplete the doubly excited state by means of SFI at variable time delays instead of just shifting its phase at a constant (near zero) time delay.

Although recent theoretical work has concentrated on the photoelectron spectrum for accessing the autoionization process, we made use of the fact that state-of-the-art optical spectrometers (*7*, *21*) attain at least an order of magnitude better energy resolution as compared with that of electron spectrometers (*22*), thus allowing for the observation of subtle changes in the spectral profile.

Upon excitation, the XUV pulse triggers the dynamic buildup of the Fano resonance by inducing an oscillating dipole moment, which in turn gives rise to the optical dipole response of the transition. Signatures in the transmitted XUV spectrum are related to the imaginary part of the frequency-domain dipole response (*7*). The time-delayed strong-field NIR pulse is then used to ionize the system, depleting the autoionizing level and ending the buildup process of the spectral line. The experimental results in Fig. 2 show the time-dependent formation of the 2s2p Fano absorption line. For the unperturbed case—in the absence of the NIR pulse as depicted in Fig. 2 (gray line)—we measured the original Fano line shape. The intensity of the 7-fs full width at half maximum (FWHM) NIR pulse was set high enough (~10^{13} W/cm^2) so that the doubly excited states were completely ionized. The dipole oscillation, and with that the resonant optical response of the atom, was thus terminated within the NIR pulse duration. Because this interruption due to SFI is considerably shorter than the lifetime of the state, we can sample the time-dependent formation of the line shape (*20*). For positive time delays τ, the terminating NIR pulse arrives after the XUV excitation pulse. When τ is small as compared with the state's lifetime of ~17 fs, the short duration in which radiation is emitted by the XUV-triggered dipole oscillation is insufficient to form a well-defined Fano line, as can be seen in Fig. 2 for τ less than 10 fs. At $\tau \approx 6$ fs, the effect of the NIR is strongest, and the spectral line is smeared out completely. When the autoionizing state is immediately depopulated after its excitation, the spectral response is mainly determined by the excitation process driven by the attosecond XUV pulse and, because of the fast termination by the NIR pulse, spans several electron volts. This result agrees with several theoretical studies (*15*, *16*) that show that the energy distribution of the electrons ejected within one third of the state lifetime (corresponding to 6 fs in the case of the 2s2p state in helium) after the initial excitation is governed by the frequency range of the excitation pulse. Now, by increasing the time delay τ between excitation and ionization, the doubly excited state has time to decay, and the interference with the direct contributions builds up; the oscillating dipole is granted more and more time to emit the optical response. This gives rise to a narrower

[1]Max-Planck-Institut für Kernphysik, Saupfercheckweg 1, 69117 Heidelberg, Germany. [2]Institute for Theoretical Physics, Vienna University of Technology, Wiedner Hauptstraße 8, 1040 Vienna, Austria. [3]Department of Physics, Kansas State University, 230 Cardwell Hall, Manhattan, KS 66506, USA. [4]Center for Quantum Dynamics, Universität Heidelberg, 69120 Heidelberg, Germany, EU.
*Present address: Stanford PULSE Institute, SLAC National Accelerator Laboratory, 2575 Sand Hill Road, Menlo Park, CA 94025, USA. †These authors contributed equally to this work.
‡Corresponding author. Email: thomas.pfeifer@mpi-hd.mpg.de

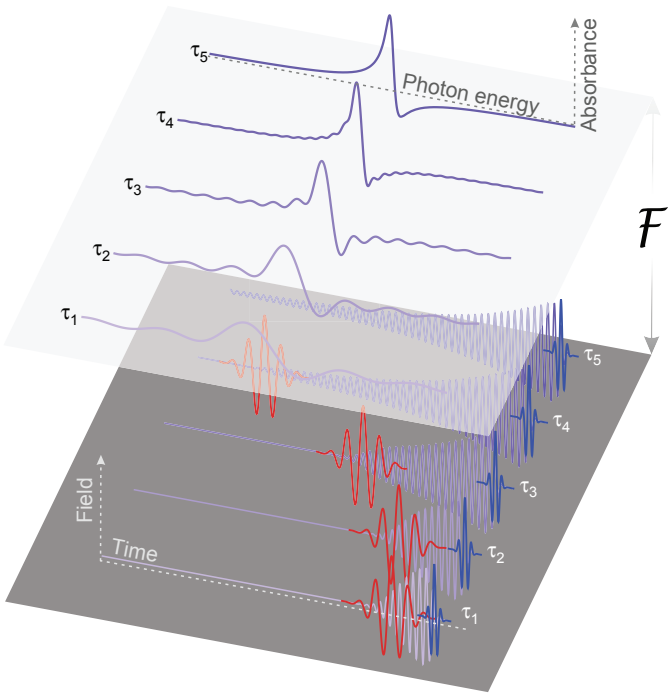

Fig. 1. Time-dependent formation of a Fano profile. The top (spectral domain) and the bottom (time domain) planes schematically show the connection between the measured absorption line shape and the temporal evolution of the dipole response (purple) for five time delays τ_1 to τ_5. After excitation of the autoionizing state by the XUV pulse (blue), the dipole decays exponentially, until the decay is terminated through complete ionization of the excited state in an intense few-cycle NIR field (red). By experimentally controlling the time delay between excitation (start) and ionization (stop), the buildup of the asymmetric Fano resonance is resolved in time.

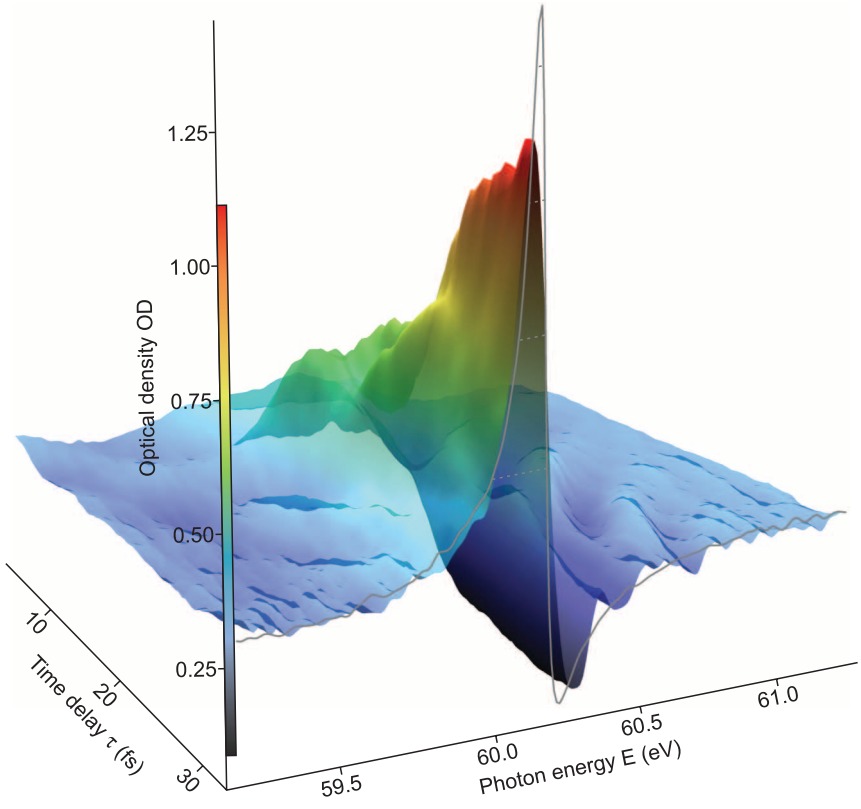

Fig. 2. Experimental observation of the Fano line formation in doubly excited helium. Transient absorption spectrum in terms of the optical density (OD) of the helium target (vertical axis) as a function of the XUV photon energy E and time delay $\tau \geq 0$ between XUV excitation and subsequent NIR ionization of the 2s2p state. For better readability, the OD values are color-coded. The reference spectrum (gray line; dashed bars indicate the OD values from 0.5 to 1.25) shows the unperturbed 2s2p line, which corresponds to the limit for $\tau \to \infty$. The experimental data were averaged over one optical cycle in order to suppress the fast oscillation of the 2s2p state absorbance due to two-photon coupling to the sp_{23+} state (*28*, *29*) and to increase the signal-to-noise ratio.

spectral line, with the details of the autoionization process encoded in it. After approximately one lifetime, at $\tau \approx 15$ fs, the Fano spectral signature is already more pronounced and continuously narrows down as the time delay is increased. For time delays substantially longer than the lifetime, the original Fano absorption profile is recovered. At the end of the delay range presented in Fig. 2, the measured line shape already closely resembles the Fano line. However, this comparison is affected by the finite experimental resolution (50 meV FWHM), which has a noticeable effect on the narrow unperturbed line. According to analytic theory (*16*, *18*, *20*), it takes roughly 100 fs for the 2s2p Fano line to develop an amplitude of 95%, and 140 fs to develop an amplitude of 99%, regarding the peak amplitude in the limit $\tau \to \infty$. Our experiment captures the most substantial changes in the line shape; further extending the time delay is not possible with our current setup.

In order to analyze our experimental observations, we solved the full two-electron Schrödinger equation of the helium atom numerically from first principles (supplementary text) (*23*). First, we verified the temporal gating mechanism by studying the residual population of the 2s2p state after SFI as a function of the time delay (Fig. 3). Although for large negative time delays the population remains unaffected, already at $\tau \approx -5$ fs less than 10% of the population remains bound because of SFI in the rising flank of the NIR pulse (peak intensity of 20 TW/cm^2). Near-complete depletion to well below 1% is first reached around $\tau \approx 4$ to 5 fs, which is in good agreement with the experimental observation. With a fall time (10 to 90% depletion) of <4 fs, the efficiency of the gate closure by the NIR pulse on time scales short as compared with the lifetime is confirmed. Moreover, as can be expected for a strong-field ionization process, the depletion of the excited state depends exponentially on the applied field strength (Fig. 3, inset).

We next compared both experiment and ab initio calculation to the analytic description of an isolated Fano resonance that is excited and depleted impulsively. The existing analytical predictions describe the photoelectron spectrum in different scenarios: either the time-dependent buildup of the continuum component of the Fano resonance (*16*, *18*, *24*), or the final distribution of photoelectrons after a sudden removal of the bound population (*20*). The four resulting photoelectron spectra are identical in the case of an isolated Fano resonance and an infinitely short gate. In order to be directly comparable with our experiment, we derived (supplementary text) an analytic expression of the transient absorption spectrum based on the description by Chu and Lin (*18*)

$$\sigma(\epsilon,\tau) \propto \mathrm{Re}\left\{1+\frac{(q-i)^2}{1-i\epsilon}\left[1-e^{-\frac{\Gamma}{2}(1-i\epsilon)\tau}\right]\right\} \quad (1)$$

Here, q and Γ are the Fano q-parameter and the resonance width, respectively, and ϵ is the

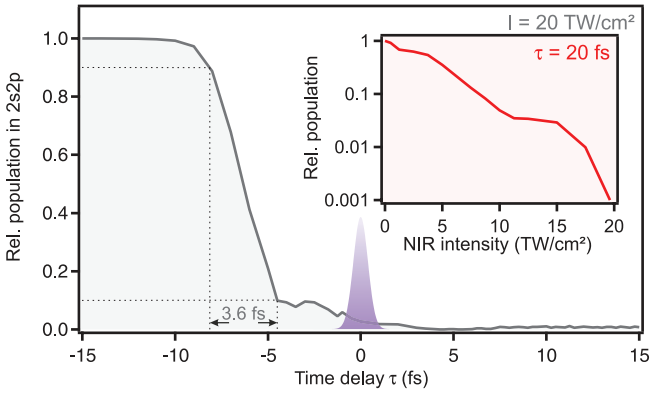

Fig. 3. Calculated occupation of the 2s2p state after SFI. For each time delay τ between the XUV and the strong NIR pulse (20 TW/cm^2), the occupation is obtained through projection onto the field-free quasi-bound state at a fixed time of 40.5 fs after the excitation by the XUV pulse. (Inset) The occupation of the 2s2p level for a fixed time delay τ = 20 fs and varying NIR peak intensity. The purple pulse indicates the arrival of the XUV pulse with respect to which the NIR is delayed by τ.

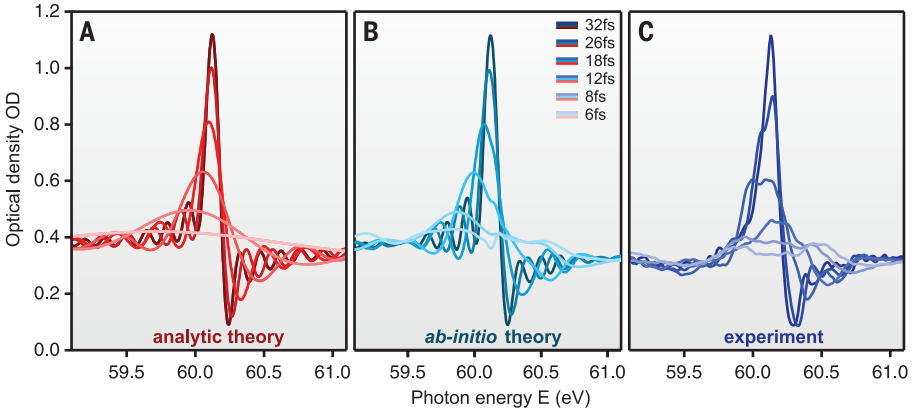

Fig. 4. Comparison between analytic theory, ab initio calculation, and experimental results for the helium 2s2p Fano line formation. (**A**) Absorption spectra calculated for a series of time delays between XUV and NIR according to the analytic expression of Eq. 1. (**B**) Numerically simulated absorption spectra for a 7-fs FWHM NIR pulse, with peak intensity of 20 TW/cm^2. (**C**) Experimentally recorded spectra. The theoretical spectral amplitudes in (A) and (B) are scaled to match the experimental peak and valley at 32 fs. Because of the finite duration of the NIR pulse in (B) and (C), the effective beginning of the line formation is not at τ = 0. Thus, the analytic spectra are shifted by 4.5 fs in time-delay in order to ensure comparability among the three data sets.

scaled photon energy [$\epsilon = 2(E - E_R)/\Gamma$, where E_R is the resonance energy]. The buildup of the Fano resonance is shown in Fig. 4 as predicted by the analytic theory (Fig. 4A) [parameters of the 2s2p line are taken from (*25*)], compared with the numerical simulation (Fig. 4B), and with the experimental data (Fig. 4C). Conceptually, the main difference is that in Fig. 4A, the depletion is treated instantaneously so that the dynamics of the quantum system are unperturbed up to the ionization event, whereas a finite-duration NIR laser pulse is applied in Fig. 4B, to model the experimental scenario (Fig. 4C). Moreover, the experimental spectra are additionally affected by a deviation of the laser pulse shape from a clean Gaussian pulse used in Fig. 4B. Still, the experimental spectra clearly resolve the buildup of the Fano resonance, validating the time-gating technique we used. The three spectra agree well with respect to their shapes and peak-to-baseline ratios, especially at later stages of the buildup (Fig. 4, darker colors), when the effect of the strong probe on the recovered line shape is small. Because the exact laser pulse profile in the experiment deviates from a Gaussian pulse used in the simulations, we cannot expect perfect quantitative agreement. Directly at the beginning of the buildup (Fig. 4, lighter colors), all spectra share a smeared-out appearance, reflecting the time-energy Fourier uncertainty relation. The ab initio calculation and the experiment agree particularly well also at these early times because they both exhibit broad wings with a similar structure, whereas the analytic spectrum is virtually flat. The discrepancy compared with the analytic theory shows that in the region of temporal overlap, the strong NIR field has a noticeable effect on the measured line shape, which is not included in the analytic model. For instance, when the NIR is present during the XUV excitation step, the 2s2p state itself is modified by the strong field (for example, by strong coupling to other states) so that the simplified sequential picture of populating (XUV) and depleting (NIR) the 2s2p state does not apply. Nevertheless, because experiment and ab initio theory agree well across the whole delay range, the physical mechanism of the time-resolved buildup of the Fano resonance is captured by the measurement. An experimental approach to reduce the pulse overlap issue would be to use NIR laser pulses with shorter duration, which could be brought closer in time to the XUV pulse without affecting the excitation.

In the future, the general method of terminating the coherent dipole response by means of laser-driven saturated ionization could be used to temporally resolve the buildup of a wide range of processes that can be tracked via their absorption spectrum. In particular for the case of overlapping resonances (*20*, *26*, *27*), this time-gating approach might be used to access the complementary time-domain information on states that are difficult to separate spectrally. Further processes of interest include the emergence of electron-electron or electron-internuclear correlations in more complex systems such as molecules, liquids, or solids and the birth of quasi-particle spectral signatures in crystals—or even more generally, the correlation dynamics in open quantum systems.

REFERENCES AND NOTES

1. H. Beutler, *Z. Phys.* **93**, 177–196 (1935).
2. U. Fano, *Nuovo Cim.* **12**, 154–161 (1935).
3. S. E. A. Orrigo *et al.*, *Phys. Lett. B* **633**, 469–473 (2006).
4. A. E. Miroshnichenko, S. Flach, Y. S. Kivshar, *Rev. Mod. Phys.* **82**, 2257–2298 (2010).
5. B. Luk'yanchuk *et al.*, *Nat. Mater.* **9**, 707–715 (2010).
6. R. Röhlsberger, H.-C. Wille, K. Schlage, B. Sahoo, *Nature* **482**, 199–203 (2012).
7. C. Ott *et al.*, *Science* **340**, 716–720 (2013).
8. P. Fan, Z. Yu, S. Fan, M. L. Brongersma, *Nat. Mater.* **13**, 471–475 (2014).
9. K. P. Heeg *et al.*, *Phys. Rev. Lett.* **114**, 207401 (2015).
10. M. Reduzzi *et al.*, *J. Phys. At. Mol. Opt. Phys.* **49**, 065102 (2016).
11. M. Kotur *et al.*, *Nat. Commun.* **7**, 10566 (2016).
12. J. Herrmann *et al.*, *Phys. Rev. A* **88**, 043843 (2013).
13. C. A. Nicolaides, T. Mercouris, Y. Komninos, *J. Phys. At. Mol. Opt. Phys.* **35**, L271 (2002).
14. Th. Mercouris, Y. Komninos, C. A. Nicolaides, *Phys. Rev. A* **69**, 032502 (2004).
15. M. Wickenhauser, J. Burgdörfer, F. Krausz, M. Drescher, *Phys. Rev. Lett.* **94**, 023002 (2005).
16. Th. Mercouris, Y. Komninos, C. A. Nicolaides, *Phys. Rev. A* **75**, 013407 (2007).
17. C. A. Nicolaides, T. Mercouris, Y. Komninos, *Phys. Rev. A* **80**, 055402 (2009).
18. W.-C. Chu, C. D. Lin, *Phys. Rev. A* **82**, 053415 (2010).
19. L. Argenti, E. Lindroth, *Phys. Rev. Lett.* **105**, 053002 (2010).
20. L. Argenti *et al.*, *Phys. Rev. A* **87**, 053405 (2013).
21. X. Wang, M. Chini, Y. Cheng, Y. Wu, Z. Chang, *Appl. Opt.* **52**, 323–329 (2013).
22. J. H. D. Eland, R. Feifel, *Chem. Phys.* **327**, 85–90 (2006).
23. J. Feist *et al.*, *Phys. Rev. A* **77**, 043420 (2008).
24. M. Wickenhauser, thesis, Vienna University of Technology, p. 53 (2006)
25. K. Schulz *et al.*, *Phys. Rev. Lett.* **77**, 3086–3089 (1996).

26. K. Meyer *et al.*, *Proc. Natl. Acad. Sci. U.S.A.* **112**, 15613–15618 (2015).
27. M. Wickenhauser, J. Burgdörfer, F. Krausz, M. Drescher, *J. Mod. Opt.* **53**, 247–257 (2006).
28. A. Kaldun *et al.*, *Phys. Rev. Lett.* **112**, 103001 (2014).
29. A. Blättermann, C. Ott, A. Kaldun, T. Ding, T. Pfeifer, *J. Phys. At. Mol. Opt. Phys.* **47**, 124008 (2014).

ACKNOWLEDGMENTS

We thank J. Feist for his work in the development of the time-dependent Schrödinger equation helium code used for the ab initio simulations. A.K., A.B., V.S., C.O., and T.P. acknowledge funding by the Deutsche Forschungsgemeinschaft (DFG) (PF 790/1-1) and the European Research Council (ERC) (X-MuSiC-616783). S.D., R.P., S.N., and J.B. are supported by the Fonds zur Förderung der wissenschaftlichen Forschung (FWF) Austria (SFB-049 NextLite, and P21141-N16) and the Wiener Wissenschafts-, Forschungs- und Technologiefonds project MA14-002. S.D. thanks the International Max Planck Research School of Advanced Photon Science (IMPRS-APS) for financial support. Ab initio calculations were performed by using the Vienna Scientific Cluster (VSC). C.D.L. and H.W. are supported by Chemical Sciences, Geosciences and Biosciences Division, Office of Basic Energy Sciences, Office of Science, U.S. Department of Energy under grant DE-FG02-86ER13491.

SUPPLEMENTARY MATERIALS

www.sciencemag.org/content/354/6313/738/suppl/DC1
Materials and Methods
Supplementary Text
References (*30*–*36*)

2 August 2016; accepted 30 September 2016
10.1126/science.aah6972

CATALYSIS

A bioinspired iron catalyst for nitrate and perchlorate reduction

Courtney L. Ford,* Yun Ji Park,* Ellen M. Matson, Zachary Gordon, Alison R. Fout†

Nitrate and perchlorate have considerable use in technology, synthetic materials, and agriculture; as a result, they have become pervasive water pollutants. Industrial strategies to chemically reduce these oxyanions often require the use of harsh conditions, but microorganisms can efficiently reduce them enzymatically. We developed an iron catalyst inspired by the active sites of nitrate reductase and (per)chlorate reductase enzymes. The catalyst features a secondary coordination sphere that aids in oxyanion deoxygenation. Upon reduction of the oxyanions, an iron(III)-oxo is formed, which in the presence of protons and electrons regenerates the catalyst and releases water.

The most efficient reduction of nitrogen- and chlorine-containing oxyanions is achieved by the microbial metalloenzymes (per)chlorate reductase and nitrate reductase during anaerobic respiration (*1*, *2*). The active sites of the two metalloenzymes are similar and allow each enzyme to reduce both nitrogen- and chlorine-containing oxyanions (Fig. 1) (*1*, *2*). Both reductases also feature extensive hydrogen-bonding networks, which facilitate the movement of protons and water about the active site and stabilize reactive intermediates (*1*–*3*). Disruption of this network in nitrate reductase via mutagenesis results in the complete loss of activity because of the low stability of high-valent Mo=O intermediates (*3*, *4*). Furthermore, positively charged residues near the active site in (per)chlorate reductase aid in the binding of perchlorate to the Mo-center (*3*). The noncovalent interactions found within the metalloenzymes play an important role in facilitating reactivity (*1*–*11*). Incorporating these interactions into transition-metal complexes may aid in oxyanion reactivity because most transition-metal systems are not capable of these reductions (*12*–*17*).

The challenge in reducing these oxyanions lies not only in their unfavorable reduction potentials but also in their low binding affinity to transition-metal centers (*12*). These inorganic oxyanions have long been touted for their weak complexation, poor nucleophilicity, and consequently their kinetic inertness toward oxidation and reduction (*12*). Therefore, harsh reaction conditions (such as low pH, high temperature, photolysis, and/or long reaction times) are required to facilitate oxyanion reduction in homogenous systems (*12*–*17*).

Inspired by the active sites of nitrate and (per)chlorate reductase, we developed a nonheme platform that incorporates the following features: (i) an earth-abundant redox-active metal center (iron) and (ii) a secondary coordination sphere that facilitates deoxygenation of substrates and high-valent iron-oxo intermediates. Previously, we reported the synthesis and characterization of a family of late, first-row transition-metal complexes [N(afa^{Cy})$_3$MOTf]OTf (M = Mn, Fe, and Co), featuring the dative (azafulvene-amine) coordination mode of the ligand and the presence of the amino-derived secondary coordination sphere (*18*–*22*). The ability of the ligand to undergo tautomerization may be a key feature during multi-electron reactions because it can facilitate proton and electron transfer between the substrate and the metal center. Furthermore, the secondary coordination sphere orients substrates binding to the metal center, as demonstrated in our nitrite reduction studies, in which a single hydrogen bond stabilized a key metal-nitrito intermediate (*21*, *22*).

The addition of tetrabutylammonium nitrite ([NBu$_4$][NO$_2$]) to 2 equivalents (eq) of [N(afa^{Cy})$_3$FeOTf]OTf (Fe^{II}-OTf; OTf, trifluoromethanesulfonate) afforded the iron(III)-oxo complex [N(afa^{Cy})$_3$FeO]OTf (Fe^{III}-O) and NO(g), which was trapped by Fe^{II}-OTf to furnish the iron(II)-nitrosyl species [N(afa^{Cy})$_3$FeNO]OTf$_2$ (Fe^{II}-NO) (*21*). Given the facile one-electron reduction of nitrite by Fe^{II}-OTf, we sought to explore the reduction of

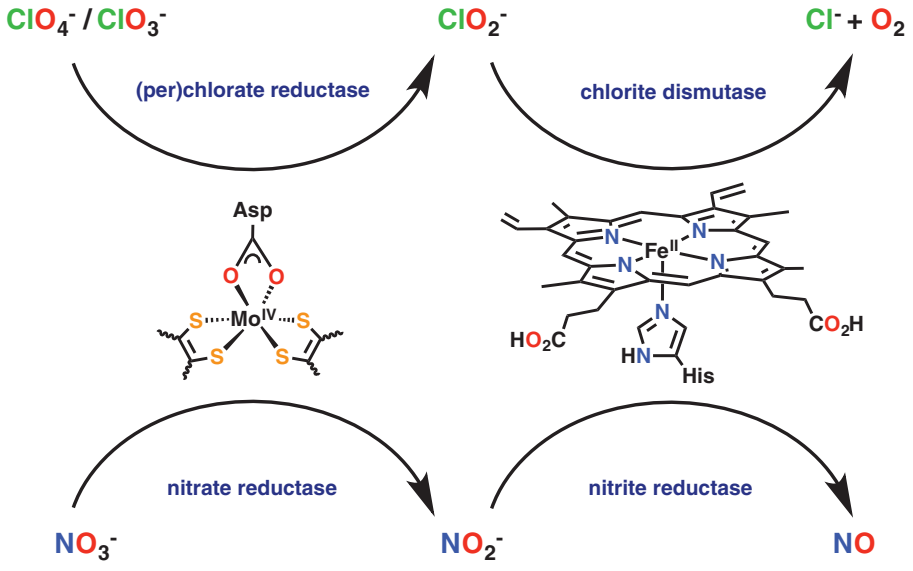

Fig. 1. Biological oxyanion reduction. The active sites of the enzymes responsible for the reduction of chlorine- and nitrogen-containing oxyanions are depicted.

School of Chemical Sciences, University of Illinois at Urbana-Champaign, 600 South Mathews Avenue, Urbana, IL 61801, USA.
*These authors contributed equally to this work. †Corresponding author. Email: fout@illinois.edu

Science
AAAS

Observing the ultrafast buildup of a Fano resonance in the time domain

A. Kaldun, A. Blättermann, V. Stooß, S. Donsa, H. Wei, R. Pazourek, S. Nagele, C. Ott, C. D. Lin, J. Burgdörfer and T. Pfeifer

(November 10, 2016)
Science **354** (6313), 738-741. [doi: 10.1126/science.aah6972]

Editor's Summary

Watching as helium goes topsy-turvy

Theorists have long pondered the underpinnings of the Fano resonance, a spectral feature that resembles adjacent rightside-up and upside-down peaks. An especially well-studied instance of this feature appears in the electronic spectrum of helium as a transient state undergoes delayed ionization. Two studies have now traced the dynamics of this state in real time. Gruson *et al.* used photoelectron spectroscopy to extract the amplitude and phase of the electron wave packet after inducing its interference with reference wave packets tuned into resonance at variable delays. Kaldun *et al.* used extreme ultraviolet absorption spectroscopy to probe the transient state while variably forcing ionization with a strong near-infrared field.

Science, this issue pp. 734 and 738

Science (print ISSN 0036-8075; online ISSN 1095-9203) is published weekly, except the last week in December, by the American Association for the Advancement of Science, 1200 New York Avenue NW, Washington, DC 20005.